CTA Coronary Labeling through Efficient Geodesics between Trees Using Anatomy Priors

Mehmet A. Gülsün[1], Gareth Funka-Lea[1], Yefeng Zheng[1], and Matthias Eckert[2]

[1]Imaging and Computer Vision, Siemens Corp. Technology, Princeton, USA
[2] Friedrich-Alexander-University, Erlangen-Nuremberg, Germany

Abstract. We present an efficient realization of recent work on unique geodesic paths between tree shapes for the application of matching coronary arteries to a standard model of coronary anatomy in order to label the coronary arteries. Automatically labeled coronary arteries would speed reporting for physicians. The efficiency of the approach and the quality of the results are enhanced using the relative position of detected cardiac structures. We explain how to efficiently compute the geodesic paths between tree shapes using Dijkstra's algorithm and we present a methodology to account for missing side branches during matching. For nearly all labels our approach shows promise compared with recent work and we show results for 8 additional labels.

Keywords: coronary labeling, shape space, tree matching.

1 Motivation and Overview

It is critical that an imaging physician report the anatomical location of pathology in a standard way to the referring physician. A principle goal of automated medical image analysis is the efficient reporting of such findings following established medical guidelines. Criteria have been established for how lesions along the coronary arteries should be reported from CT angiography (CTA) [1,8]. The number of coronary labels varies in different standards but there is agreement on the major labels. The AHA established a standard 15 segment model in 1975 [1]. Our model follows more closely the more recent and more complete models of [8,6]. The physician generally knows which coronary segment contains a lesion but it is time consuming to label images when more than a few labels must be applied. So the goal of automatic coronary labeling is not to inform the physician of the anatomy but to speed the preparation of a report.

In order to label the coronaries, our approach will leverage both geometric and topological information to define the correspondence between a labeled model and unlabeled data. We only consider the centerlines of the coronaries and not the coronary lumen. Most prior work labeling vascular or airway trees extracts an abstract graph that captures the topology of the tree but uses limited or no geometric information. A graph matching algorithm is then run to define the best correspondence between nodes in the model and in the unlabeled graph

P. Golland et al. (Eds.): MICCAI 2014, Part II, LNCS 8674, pp. 521–528, 2014.

[2,7]. This is a natural approach when attempting to label coronaries in 2D X-ray angiograms where the 3D geometry has been lost as in [2,7].

Recent work by [9] labels 3D CTA in 2 steps based on an anatomical model derived from [1]. First, a reduced coronary model is rigidly aligned using a point-set registration method and labels for the major branches are assigned based on proximity. Second, the side branches are labeled based on iteratively reducing a cost function which penalizes unlabeled centerline points. Our approach can handle more general trees and so could be applied to other anatomy. In the results section, we compare our results with theirs.

Our solution builds on the recent work defining unique geodesic paths between trees [4], specifically, the proposed Quotient Euclidean Distance (QED) metric to compute in general *unique* natural and continous geodesic paths between tree-shapes by concatenating local tree deformations [4]. The paths are defined in a high dimensional space that captures the topology and geometry of the tree. The QED geodesic was previously applied to the computation of an average airway tree [3] and to matching airway trees [5].

The main contributions of this paper are 1) the practical definition of the 3D QED geodesic space for coronary trees based on automatically detected cardiac anatomy, 2) an efficient computation of the QED geodesic using Dijkstra's algorithm, 3) the use of a coronary territory prior to augment the shape and topology information, 4) explicit explanation of our heuristic in the QED framework to handle missing side branches. We first explain the QED metric and then explain its application to coronary labeling. We then present strong coronary labeling results on manually and automatically detected coronary trees.

2 Method

In our method, we label a given target coronary tree by finding a minimum cost tree-shape deformation from a coronary atlas model. We define the deformation cost between two coronary trees as the weighted sum of the QED distance between them and a second cost term based on the likelihood of the assigned labels to the target coronary branches which is computed from the spatial distribution of coronaries over the heart surface.

As in [4], our vessel tree representation consists of a description of the branch topology and the shape of the branches which together correspond to a point in high dimensional space X. We represent a tree-shape as a pair (T, f) consisting of first, an ordered binary tree $T = (B, r)$ with branches B and a root point r which together represent the tree topology, and second, branch attributes f that map each branch in B to n landmark points sampled along the branch geometry. In this tree-shape model, tree-shapes with non-binary topology are represented via binary trees with collapsable zero-length internal branches. Figure 1c makes it clear that the same tree-shape may correspond to different points in our space.

Our goal is then to find a geodesic path between two such tree-shape points. However, geodesic paths in such a high dimensional space do not necessarily give continuous and natural deformations, since these geodesic paths do not

contain equivalent tree-shapes with different binary representations, Figure 1a. Therefore, it is important to identify all the points in this space representing the same tree-shape. In [4], a quotient space $\tilde{X}$ is defined to glue all points in the space X that correspond to the same tree-shape. In the quotient space, two tree-shape representations are considered to be identical, after collapsing their zero-length branches, if the corresponding combinatorial, ordered, rooted and attributed trees are exactly the same, Figure 1c. The geodesic metric in this space is called the Quotient Euclidean Distance (QED) where the distance between glued points corresponding to same tree-shape is considered to be zero.

The QED geodesic between two tree-shape points in quotient space is the path with minimum distance cost over all possible paths, Figure 1b, c. The distance cost $d(x, y)$ between two tree-shape representations x and y is defined as the L2 norm of the deformation costs between corresponding branches in two tree-shapes. This branch deformation cost is computed as the sum of the Euclidean distance between landmark points of the two branches with their first points aligned. The cost of removing a branch is same as deforming it to a zero length branch.

In general, finding geodesic paths in QED space is computationally very expensive. One algorithm for computing QED geodesic is to explore all paths following all possible internal topology changes and choose the one with minimum cost among them. However, the number of all possible internal topology changes grows exponentially with the total number of internal branches of the tree-shape. In fact, some sequences of internal topology changes may have a cost larger than the geodesic cost. In order to eliminate redundant paths containing such sequences, we propose to use Dijkstra's shortest path algorithm which is guaranteed to compute the shortest path when the graph metric is non-negative. We construct a graph $G = (V, D)$ where each node V in this graph corresponds to a tree-shape and are connected with edges D. An edge connecting two nodes with identical tree-shape is assigned with zero cost and an edge connecting two nodes with different tree-shapes is assigned with the minimum of distance costs between all possible pairs of different tree-shape representations of the two tree-shapes, $\tilde{d}(\tilde{T}_1, \tilde{T}_2)$ in Figure 2b. Note that the cost of an internal topology change is the removal cost for the corresponding internal branch. The edge costs are computed only when they are needed in Dijkstra's propagation for efficiency.

Major side branches of the coronaries could be missing in a sample due to anatomical variation, pathology, image acquisition issues, or segmentation errors. One major contribution of this work is to consider equivalent partitioned representations of source and target tree-shapes to account for missing side branches, Figure 2a. Given two tree-shape representations, we collapse all zero-length branches and merge the branch geometry of consecutive branches without bifurcations to form a single branch in a new tree representation. If the two new representations are exactly the same, we consider these two tree-shape representations to be equivalent. This definition of identical tree-shapes allows for partitioning a tree-shape branch into one or more consecutive branches in B to naturally account for missing side branches, Figure 2a. Specifically, we compute

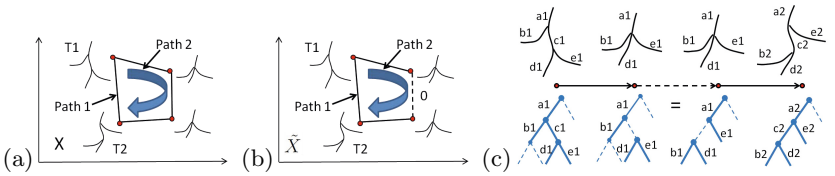

Fig. 1. (a) T1 and T2 are tree-shape points in a high dimensional space. A third tree-shape can be obtained by removing the internal branch of T1. Path 1 is the geodesic path in the original space X. Path 2 is a continuous deformation but not a minimum cost path. (b) In Quotient Space $\tilde{X}$, Path 2 is a feasible geodesic path because two different representations of the same tree-shape are allowed along the path with zero cost between them. Note that Path 2 goes through an internal topology change. (c) Tree-shapes (top) and their representations (bottom) along the geodesic Path 2.

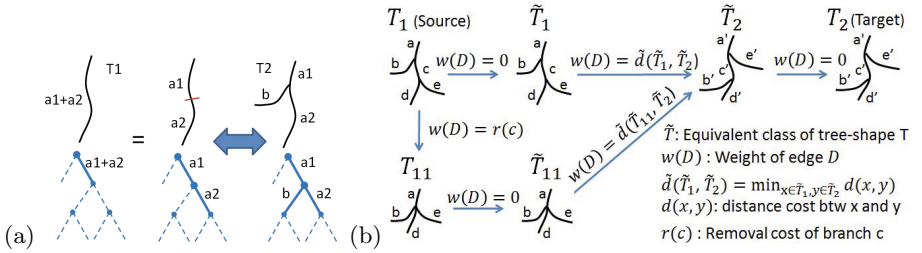

Fig. 2. (a) T1 has a missing side branch. Its main branch is partitioned and mapped onto the equivalent second representation (middle) with two consecutive branches. This allows the side branch to *grow* naturally along the geodesic path. (b) Our constructed graph for Dijkstra's algorithm to compute QED geodesic from T_1 to T_2.

QED geodesic between all possible partitioning of source and target tree-shape branches in to at most three equal length polylines. Note that the tree-shape partitioning is a heuristic step of our algorithm that uses the QED tree-space.

It is not practical to apply QED to arbitrary trees embedded in 3D space because it requires considering all possible orderings of the child branches. For the coronaries, we can order the branches based on their position relative to the surface of the heart. Specifically, we automatically detect all four cardiac chamber using the method of [12,10] and use them to find branch orderings of right and left coronary trees relative to the right and left ventricles, respectively.

In addition, since we know the underlying cardiac anatomy, we can use it to compute the likelihood of where a particular coronary branch tends to lie. We add a second cost term to our tree-shape deformation cost in addition to the traditional QED distance. This second term accounts for the cost of assigning a label to a specified branch on the target tree based on its location over the heart territory. The likelihood for each branch is computed from the spatial distribution of hand annotated coronary trees aligned using a thin-plate spline (TPS) defined by the detected cardiac chamber and pericardium models, Figure 3.

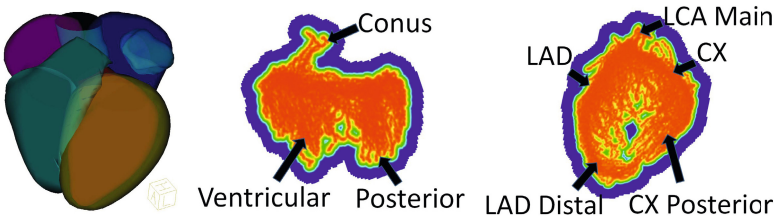

Fig. 3. (a) Automatically detected four chamber models are used for aligning coronary trees with TPS interpolation. (b) Right and (c) left coronary territories with certain regions depicted. Red indicates high probability, blue low probability.

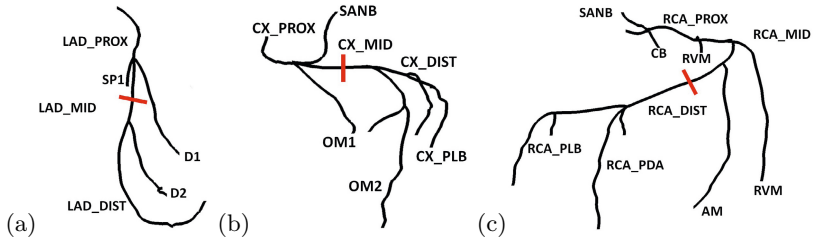

Fig. 4. a) The left coronary artery (LCA) has 14 labels: left main (LM), three segments of the left anterior descending (LAD): proximal (LAD_PROX), mid (LAD_MID), and distal (LAD_DIST), diagonals (D1, D2), septal perforating (SP1), b) three segments of the circumflex (CX): proximal (CX_PROX), mid (CX_MID), and distal (CX_DIST), sinoatrial nodal (SANB), posterolateral (CX_PLB), and obtuse marginals (OM1, OM2). c) The right coronary artery (RCA) has 9 labels: three segments of the right coronary artery: proximal (RCA_PROX), mid (RCA_MID), and distal (RCA_DIST), sinoatrial nodal (SANB), conus (CB), right ventricle marginal (RVM), acute marginal (AM), posterolateral (RCA_PLB), and posterior descending (RCA_PDA). Proximal and distal subtrees are separated by red lines.

We achieve labeling an unseen coronary tree by propagating labels from a coronary atlas model along the geodesic path computed between them. Our coronary atlas model has a fixed topology described by [6] and we use mean branch shapes computed over the most complete 10 coronary trees in the training set. Figure 4 shows our coronary model in 3D space. Our coronary model is an instance of both right-dominant and co-dominant circulation which are seen in 92% of the population [6]. This is why we excluded the CX posterior descending artery in our coronary model. The ramus intermediate branch is also excluded.

The computational cost of our matching increases with the size of the trees. However, coronary arteries may have more generations than what is practical with the QED metric. Therefore, we partition RCA tree, LAD and CX subtrees into proximal and distal parts by maximizing the likelihood of their locations on coronary territory. Figure 4 shows the proximal and distal parts separated by red lines. Each subtree is labeled separately.

Table 1. Label assignments as a percentage for those branches with the most mislabels

RVM	RVM (88%), CB (3%), None (9%)
AM	AM (73%), RVM (19%), None (8%)
RCA_SANB	RCA_SANB (80%), None (20%)
OM2	OM2 (83%), CX_PLB (8%), None (9%)
D2	D2 (83%), LAD_MID (12%), None (5%)

3 Results

Our QED geodesic implementation supports 3 generations. We keep a table for quick look-up of equivalence classes of tree shapes. Our parallelized implementation with OpenMP computes the QED geodesic between 2 tree-shapes with at most 2 internal branches in 30 seconds on a Quad Core Xenon 3GHz processor and 8 GB RAM. Labeling both left and right coronary trees takes 3 minutes.

We assume that the left main (LM) and the proximal branches of the RCA, LAD and CX always exist. To make the input centerlines suitable for use in our QED implementation, each proximal and distal part of RCA, LAD and CX trees were preprocessed by iteratively pruning their shortest branches until they had a maximum three generations.

We evaluated our method for right and co-dominant dominant cases using leave-one-out cross-validation where the coronary spatial distribution is recomputed for each training set. We experimentally chose the best weighting term between QED distance and label assignment likelihood terms. The ramus branch was removed from the entire test set and should be treated separately. We used expert annotated coronary centerlines in 37 CTA datasets. We automatically detected the pericardium mask and four chamber models to define our coordinate system [10,12]. Each of the ground truth centerlines was labeled according to [6] where the same label of the side branch is used to label its children. For evaluation, labels corresponding to pruned branches are recorded as part of the missed results. Figure 5 illustrates the matching between the model and a test coronary tree. We calculated the overlap measures between automatic and expert annotated labels for each branch that exists in our coronary model. Branches that exist in our model but that are not labeled by the algorithm are counted as mislabeled. Figure 6 compares our results to those of [9]. Note that the two test datasets are different and so the results are suggestive rather than being directly comparable.

We evaluated our labeling method on 20 patient cases of automatically detected coronary centerlines [11] that combines a model driven approach for the three major coronary arteries with a data driven approach for the side branches and distal parts of the main branches. Because the method of [11] knows which of the three main coronary branches it has recovered, the label of these branches is known as part of the segmentation. However, in order to show the generality of our approach to labeling, these known labels are ignored and we present a method that can label the coronary tree without any known labels.

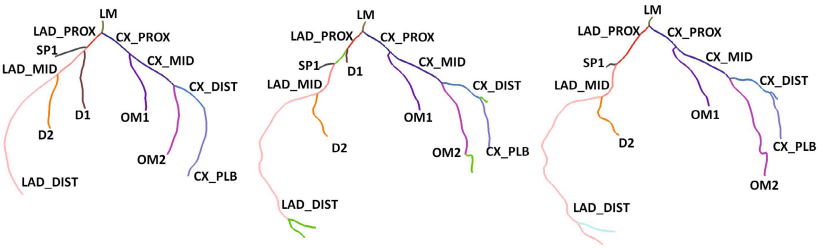

Fig. 5. A sample test tree (right) matched to our model (left). An intermediate tree along the geodesic path is shown in the middle. Each color corresponds to a label. New grown branches are depicted in green. The first diagonal is missing in the test tree.

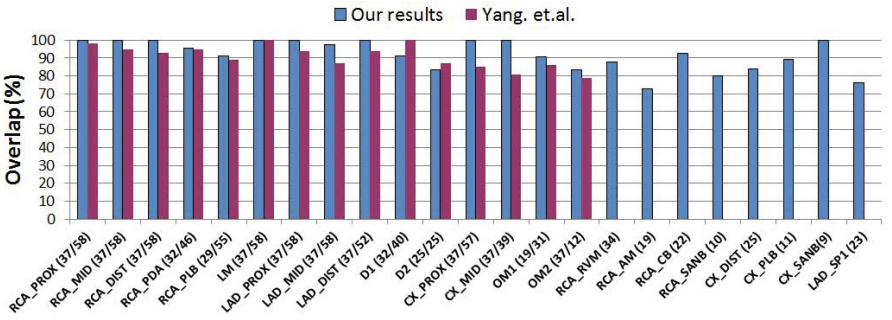

Fig. 6. Comparison of our overlap measures to Yang et. al. [9]. Total count of each branch is depicted next to its label for our and their test set, respectively. Our results for branches that were not part of their results appear as single columns.

Our success rate is 95% for the right coronary and 93% for the left coronary for hand annotated centerlines, and 87% for the right coronary and 86% for the left coronary for detected centerlines. Without the anatomical location prior, the results for the hand annotated centerlines decrease to 92% for the right coronary and 89% for the left coronary. In the case of the automatically detected coronary branches, there are 14 instances of false positive detections which explain our reduced labeling performance. Specifically, in 51% of these cases,the false positives are incorrectly given a label and the assigned label depends on the location.

4 Conclusion

We have presented an efficient method that determines a geodesic path between tree shapes in order to propagate labels from a standard model of the coronary arteries to unlabeled coronary centerlines. Our approach adapts the framework of [5] to work on the detected surface of the heart. For most of the labels assigned by [9] our approach produces equivalent or better results. However, our approach can handle more general tree structures and we have shown results on 8 additional labels. Also, we show results for coronary trees produced by an automatic

detection algorithm. Additional contributions include the efficient computation of the QED geodesic using Dijkstra's algorithm, the use of a coronary territory location prior, and an explicit description of how to support missing side branches in the QED framework. However, the major limitation of our approach is the computational complexity of QED for trees with many generations. In future work, we will consider having multiple coronary models in order to handle left dominant circulation (approximately 8% of the population [6]) or the rare cases where the left main trifurcates into a ramus intermedius, LAD and CX [6].

References

1. Austen, W.G., Edwards, J.E., Frye, R.L., et al.: A reporting system on patients evaluated for coronary artery disease. Report of the ad hoc committee for grading of coronary artery disease, council on cardiovascular surgery, American Heart Association. Circulation 51, 5–40 (1975)
2. Ezquerra, N., Capell, S., Klein, L., Duijves, P.: Model-guided labeling of coronary structure. IEEE Trans. on Medical Imaging 17(3), 429–441 (1998)
3. Feragen, A., Hauberg, S., Nielsen, M., Lauze, F.: Means in spaces of tree-like shapes. In: ICCV, pp. 736–746 (2011)
4. Feragen, A., Lauze, F., Lo, P., de Bruijne, M., Nielsen, M.: Geometries on spaces of treelike shapes. In: Kimmel, R., Klette, R., Sugimoto, A. (eds.) ACCV 2010, Part II. LNCS, vol. 6493, pp. 160–173. Springer, Heidelberg (2011)
5. Feragen, A., Lo, P., Gorbunova, V., et al.: An airway tree-shape model for geodesic airway branch labeling. In: Third MICCAI Workshop on Mathematical Foundations of Computational Anatomy (2011)
6. Fiss, D.M.: Normal coronary anatomy and anatomic variations. Applied Radiology 36(1), 14 (2007)
7. Haris, K., Efstratiadis, S.N., Maglaveras, N., Pappas, C., Gourassas, J., Louridas, G.: Model-based morphological segmentation and labeling of coronary angiograms. IEEE Trans. on Medical Imaging 18(10), 1003–1015 (1999)
8. Raff, G.L., Abidov, A., Achenbach, S., et al.: SCCT guidelines for the interpretation and reporting of coronary computed tomographic angiography. J. of Cardiovascular Computed Tomography 3(2), 122–136 (2009)
9. Yang, G., Broersen, A., Petr, R., et al.: Automatic coronary artery tree labeling in coronary computed tomographic angiography datasets. Computing in Cardiology 38, 109–112 (2011)
10. Zheng, Y., Barbu, A., Georgescu, B., et al.: Four-chamber heart modeling and automatic segmentation for 3-D cardiac CT volumes using marginal space learning and steerable features. IEEE Trans. on Medical Imaging 27(11), 1668–1681 (2008)
11. Zheng, Y., Tek, H., Funka-Lea, G.: Robust and accurate coronary artery centerline extraction in CTA by combining model-driven and data-driven approaches. In: Mori, K., Sakuma, I., Sato, Y., Barillot, C., Navab, N. (eds.) MICCAI 2013, Part III. LNCS, vol. 8151, pp. 74–81. Springer, Heidelberg (2013)
12. Zheng, Y., Tek, H., Funka-Lea, G., Zhou, S.K., Vega-Higuera, F., Comaniciu, D.: Efficient detection of native and bypass coronary ostia in cardiac CT volumes: Anatomical vs. pathological structures. In: Fichtinger, G., Martel, A., Peters, T. (eds.) MICCAI 2011, Part III. LNCS, vol. 6893, pp. 403–410. Springer, Heidelberg (2011)